Control of semiconductor quantum dot emission intensity and polarization by metal nanoantennas

V. I. Kukushkin, I. M. Mukhametzhanov, I. V. Kukushkin, and V. D. Kulakovskii
Institute of Solid State Physics, RAS, 142432 Chernogolovka, Moscow district, Russia

I. V. Sedova, S. V. Sorokin, A. A. Toropov, and S. V. Ivanov
Ioffe Physical-Technical Institute, Russian Academy of Sciences, Polytekhnicheskaya 26, 194021 St. Petersburg, Russia

A. S. Sobolev
Moscow Institute for Physics and Technology (State University), 141700 Institutsky Pereulok, 9, Dolgoprudny, Russia
and Kotel'nikov Institute of Radio Engineering and Electronics, RAS, 125009, Mokhovaya Street 11/7, Moscow, Russia
(Received 22 May 2014; revised manuscript received 23 October 2014; published 18 December 2014)

We have studied the amplified emission properties of nanoislands with CdSe quantum dots in ZnSe/CdSe/ZnSe heterostructures surrounded by metallic antennas. It has been found that variations of the optical antenna length give rise to periodic amplification of the integral emission intensity. The period of the discovered oscillations corresponds to the wavelength of the surface plasmon-polariton mode propagating in the metallic antenna. The nature of observed periodicity was confirmed by results of numerical simulations for linear antennas. It has been established that the velocity of surface polaritons depends not only on the parameters of the dielectric constants of the metal and of the semiconductor substrate but also on the width of the metallic antenna. The influence of antenna antisymmetry (its helicity) on selective amplification of the degree of circular polarization of photoexcitation has been investigated. We found that plasmon-polariton standing waves induced in *S*-type (curved) antennas by circularly polarized light, which was used for quantum dot photoexcitation, result in enhanced polarization selectivity of the quantum dot emission. The selectivity of the polarization of photoexcitation is a periodic function of the helical antenna length.

DOI: 10.1103/PhysRevB.90.235313 PACS number(s): 78.67.−n, 33.90.+h, 33.55.+b

I. INTRODUCTION

The emission, detection, and amplification of electromagnetic waves in the radio-frequency range by different antennas have been well studied and detailed in numerous textbooks [1,2]. However, the emission peculiarities of nano-objects with characteristic sizes close to a nanometer (for instance, emission of a single molecule) and the feasibilities of emission control are still problems of profound importance in modern nano-optics [3,4]. Solutions to these problems would enable us to achieve significant emission amplification coefficients for nano-objects as well as to control their emission directivity. At the low-frequency range (10^7–10^9 Hz), metals can be considered to be nearly perfect mirrors; in contrast, at high frequencies corresponding to the visible range ($\sim 10^{15}$ Hz), metals exhibit intensive transmission and absorption of light. Therefore, the ideas on antenna design which have been sufficiently well developed in the radio-frequency range should essentially be revised for application in nano-optics, with a view to control emission from nano-objects.

As was shown by Purcell [5], emission intensity and directivity can be significantly changed by varying the molecular environment. The conversion of the emission from molecules and quantum dots into surface plasmon polaritons on an infinite metal plane and the interaction between them was studied theoretically [6,7]. In a number of experiments the enhancement of spontaneous emission by plasmonic nanocavities [8] was demonstrated. For instance, in Ref. [8] the enhancement of spontaneous emission in plasmonic nanocavities was studied for the cavity mode localized in the gap between the Ag substrate and Ag nanowire, whose diameter or length did not affect the enhancement efficiency. Other approaches to create localized plasmons may involve nanocavities formed by Ag-plated diamond nanocylinders [9] to enhance the single-photon emission or noble-metal nanospheres for surface-enhanced Raman spectroscopy [10]. The applications of Purcell's idea are also well known and extensively used in microwave devices [11,12]. For instance, placing a point source (a Gunn diode or an impact ionization avalanche transit time diode with a size of about 5 μm) into a cavity connected to a waveguide leads to appreciable power amplification and ensures emission directivity [13–15]. Similarly, the intensity and directivity of a single-molecule emission can be changed by placing the molecule into a cavity with a characteristic size of a single wavelength. The emission properties of the molecule can be influenced by creating an environment that prevents the propagation of light. Some well-known examples are one-, two-, and three-dimensional photonic crystals prepared in the form of periodic dielectric structures using the effects of multibeam interference [16–18]. Such photonic crystals can increase the lifetime of the excited state by many orders of magnitude.

Besides the use of cavities and photonic crystals, which are fairly intricate devices, the simplest way to manipulate the emission of single molecules is the design and optimization of metallic antennas capable of changing emission power and direction. The first trivial idea about the application of metallic antennas in the optical range is to use a dipole antenna with a length equal to a half of the wavelength of light and a gap which is much smaller than the wavelength. Such attempts have recently been made [19–23] and have revealed that the electric field in the gap is amplified 10–20 times.

The authors of Ref. [19] used the simplest λ half-dipole antenna so that the current was minimal at the antenna ends and maximal in the gap between the two λ quarter-antenna

parts. The amplified amplitude of the electromagnetic field in the gap was detected using a technique based on the properties of nonlinear transformation of a powerful femtosecond pulse into a wide band of practically white light, the intensity of which reflected the efficiency of the nonlinear transformation and allowed estimating the amplitude of the electromagnetic field in the antenna gap.

In the present work the emitting nano-objects are nanoislands (mesas) of ZnSe/CdSe quantum dots (QDs) with a characteristic size of 3–10 nm. We have studied the effect of metal optical nanoantennas on the intensity and polarization of ZnSe/CdSe/ZnSe QDs emission under excitation by an Ar-ion laser at 488-nm wavelength. Both linear and helical antennas have been studied. The oscillations of the enhancement factor as a function of the antenna length have been established in both linear and helical antennas, and it is demonstrated that the period of observed oscillations corresponds to the wavelength of the surface plasmon-polariton mode propagating in the metallic antenna. It has been found that the helical antennas also induce pronounced polarization dichroism with respect to photoexcitation by circularly polarized light.

This paper is arranged as follows. The experimental technique and sample fabrication are discussed in Sec. II. The effects of linear and helical antennas on QD emission are discussed in Secs. III and V, respectively. In Sec. IV we present and discuss the numerical simulation results for linear antennas.

II. EXPERIMENTAL TECHNIQUE AND SAMPLES

The properties of optical nanoantennas made of silver and gold were investigated using emissions from nanoislands (mesas) with 10–40 CdSe QDs confined between ZnSe layers. The distance between QD layers and the top of the structure was 15 nm. The QD nanostructures were grown by molecular-beam epitaxy (MBE) on GaAs(001) substrates in a standard MBE mode. The nominal thickness of deposited CdSe was around three monolayers, which resulted in strain-induced self-formation of CdSe QDs with an average density of $\sim 10^{11}$ cm^{-2}. Electron-beam lithography (JEOL-JSM-7001F) and liquid etching were used to fabricate single mesas with a characteristic lateral size of $d = 50$–150 nm and a height of 50 nm across the surface of the ZnSe/CdSe/ZnSe heterostructure. Since the characteristic QD density in the heterostructures was 10^{11} cm^{-2}, the number of QDs in the mesa was varied from 5 to 60. In order to reduce the influence of the fluctuation of the QD number in the mesas, it was necessary to use mesas ranging in size from 70 to 100 nm, which enabled fabrication of antennas with gap $D = 110$–140 nm (see the bottom part of Fig. 1). A further increase in the mesa size resulted in significant attenuation of the antenna enhancement effect due to the unavoidable increase of the antenna gap. Thus, the main research object was a mesa with a typical size $d \sim 100$ nm which was embedded in a metallic (silver or gold) nanoantenna with thickness $h = 50$ nm. The width w varied from 100 to 300 nm, and the length l was in the range from 60 to 2000 nm. In fact, h is the thickness of the metal film, from which the planar nanoantenna is patterned. Besides rectilinear antennas, helical (S- and Z-type) antennas

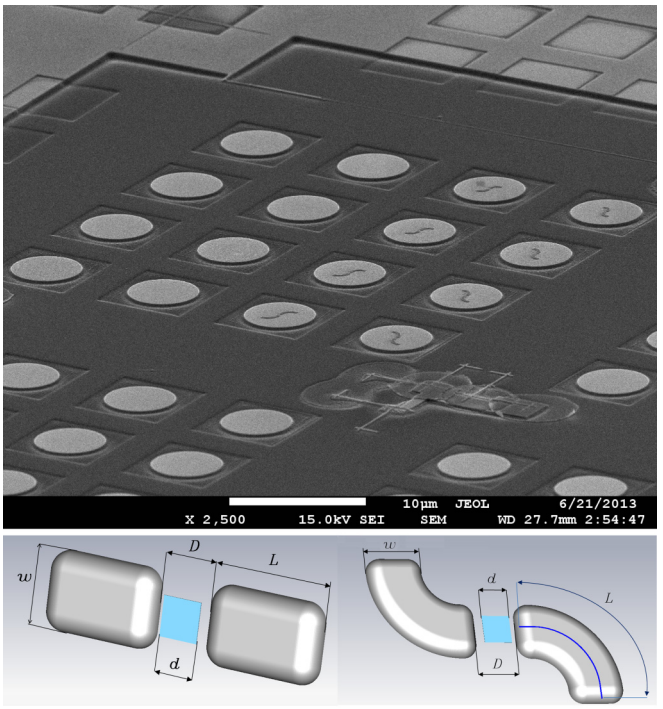

FIG. 1. (Color online) (top) View of part of the structure used for the investigations. The structure was divided into substructures, each of which comprised 16 mesas (4×4 structure seen in the figure) with QDs. The distance between the mesas was 10 μm, so that the substructure size was 50×50 μm. In each substructure two of the 16 mesas had no nanoantennas and were used for comparison. The remaining 14 mesas were embedded into nanoantennas with different geometric parameters. (bottom) The schematic representation of the geometry parameters for both linear and S-type antennas. For S-type antennas L is the average length between the outer and inner edges of one antenna arm.

were also fabricated to study selective enhancement of circular polarization of photoexcitation.

All the measurements were made at room temperature using a Raman microscope that ensured a spatial resolution of about 1 μm and spectral resolution of 0.1 nm and allowed plane scanning of the structures with a 0.1-μm step. All the structures in question were divided into substructures, each of which comprised 16 mesas with QDs. The distance between the mesas was 10 μm so that the substructure size was 50×50 μm (see Fig. 1). In each substructure 2 of the 16 mesas had no nanoantennas and were used for comparison. The remaining 14 mesas were embedded in nanoantennas with different geometric parameters. A typical structure consisted of 16 substructures, which enabled us to obtain about 200 experimental points by varying, for instance, the length of the optical nanoantenna. Some structures were used to study the properties of curved antennas: pairs of antennas with clockwise and counterclockwise curving were drawn for immediate comparison of the properties of the antennas upon excitation with left- and right-circularly polarized light.

Analysis of the QD emission amplified by the nanoantennas involved calculation of the integral emission intensity (integrated over the whole spectral range as well as over the area

corresponding to the mesas with QDs). The effects of selective amplification induced by the curved antennas in the cases of different circular polarization of light were investigated using polarized laser photoexcitation with a fixed wavelength (488 nm); however, the emission from the mesas was taken without any polarizers.

Note that special attention was given to avoiding an overlap between the metallic antenna and the mesa. It was established that with very close (both top and lateral) proximity of the metal to the QDs (less than 10 nm) the intensity of QD emission drops considerably (by orders of magnitude). This effect is related to the phenomena described by Sommerfeld, who calculated the emission of a dipole oscillator in the vicinity of a metal plate [24–26]. Therefore, all the gaps between the QDs and mesas in our structures exceeded 20 nm when the quenching of QD emission was negligible.

An analysis of the degree of circular polarization ρ_c generated by nonpolarized photoexcitation revealed that all the resonant features broadened and practically disappeared due to the significant width of the emission line of the QDs at room temperature. In addition to silver nanoantennas, we also used gold ones and, for reference, investigated the properties of nanoantennas deposited on glass substrates, with the emitting objects being organic molecules (such as carotene and rhodamine 6G).

III. EFFECT OF LINEAR ANTENNAS

Figure 2 illustrates the emission spectra of a single mesa (see insets in Fig. 3) with ZnSe/CdSe QDs (mesa diameter $d \sim$ 100 nm) measured after photoexcitation generated by 488-nm circularly polarized light (with left and right polarization). It is seen that in the absence of metallic nanoantennas the QD emission is not sensitive to the sign of the circular polarization. It was also found that the orientation of the linear polarization plane of the exciting light did not affect the intensity and shape of the emission spectrum when the number of QDs in the islands was more than 20 (realized with mesas with d equal to 100 nm).

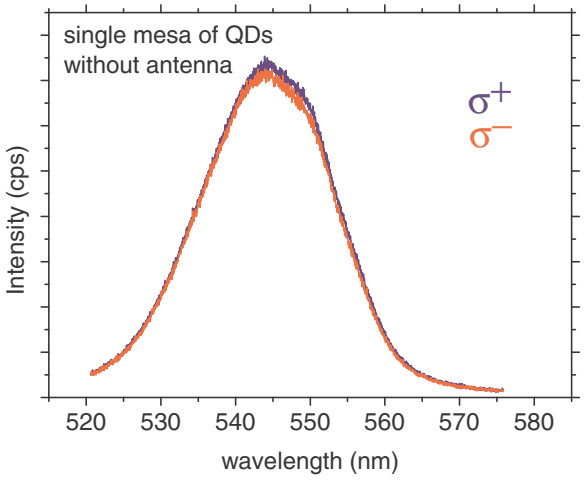

FIG. 2. (Color online) Emission spectra of a single mesa with CdSe/ZnSe QDs under photoexcitation by a laser ($\lambda = 488$ nm) with left and right circular polarization.

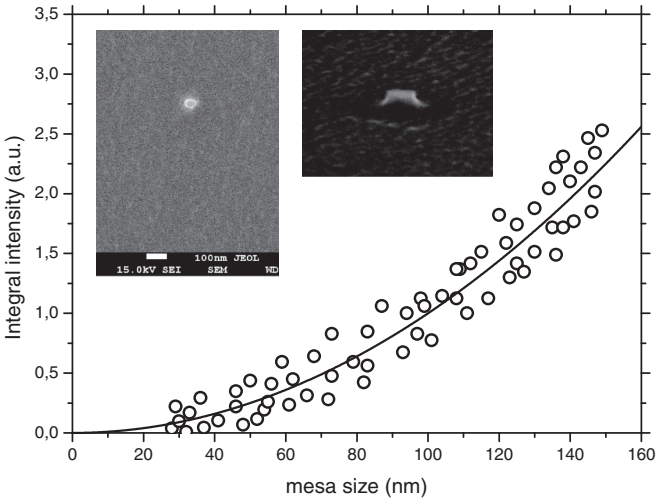

FIG. 3. Dependence of the integral emission intensity of single mesas on mesa size. The insets show photos of single mesas with $d \sim 80$ nm obtained with an electron-beam microscope.

The integral emission intensity of single mesas with ZnSe/CdSe QDs was studied as a function of mesa size, which is shown in Fig. 3. Besides the obvious quadratic mesa diameter dependence of the integral emission intensity, from this dependence it also follows that with mesa sizes less than 60 nm, the integral intensity fluctuations increase considerably and reach 50%–90% for mesas with $d = 30$ nm, which is due to strong variations of the number of QDs in the mesa (this number is reduced down to 1, 2, or 3). Hence, reliable analysis of the effects of ZnSe/CdSe QD emission intensity amplification using nanoantennas requires mesas with d from 70 to 100 nm or more. Given such mesa sizes, the antenna gap with an emitting nano-object increases up to 120–150 nm, which undoubtedly limits the amplitude of emission intensity amplification but provides reproducible results.

Figure 4 shows the photos of experimentally realized characteristic structures (linear metallic nanoantennas with gaps containing mesas with QDs) obtained using an electron-beam microscope. The height of the nanoantennas and mesas is 50 nm, with the antenna length varying from 50 to 2000 nm. The structure sets are prepared and investigated for different antenna widths (100–300 nm) as well as different mesa sizes (80–120 nm) and antenna gaps (120–200 nm).

Figure 5 shows the emission amplification ratio $\gamma = I_{\mathrm{QD,ant}}/I_{\mathrm{QD},0}$ of QDs embedded in silver linear antennas as a function of antenna length. Here $I_{\mathrm{QD,ant}}$ and $I_{\mathrm{QD},0}$ are the emission intensities of the mesa with and without metal antennas, respectively. The measurements were made using light with linear polarization along the antenna, $w = 200$ nm, $D = 150$ nm, and mesa size $d = 100$ nm. It is seen that $\gamma(l)$ is an oscillating periodic function of antenna length, and at the oscillation maximum it can reach a factor of 6, while the oscillation period for the indicated antenna parameters is $L = 210$ nm. Besides the main resonances denoted by number $N = 1,2,3$, and 4, extra amplification maxima were observed at half periods ($N = 1/2$) and at quarter periods ($N = 1/4$).

We attribute the observed periodicity to the effect of antenna emission amplification with the formation of standing

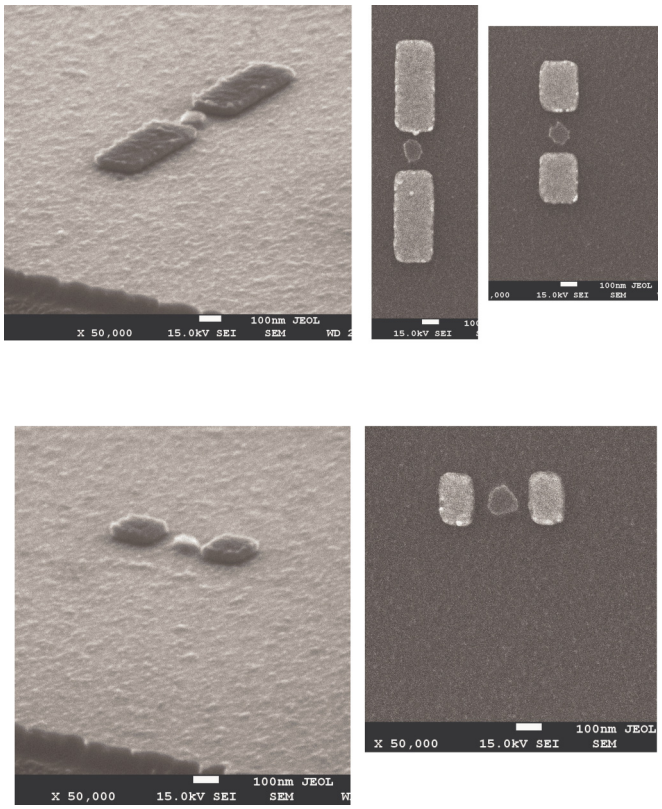

FIG. 4. (Color online) Typical photos of structures with linear metallic nanoantennas obtained using an electron-beam microscope.

waves in the metallic antenna and ascribe them to the surface plasmon-polariton modes, the dispersion of which is determined by the dielectric constant parameters of the metal and the semiconductor substrate. For a wavelength of light $\lambda_0 = 488$ nm (energy 2.54 eV) the parameters of the real and imaginary parts of the silver dielectric constant are $\epsilon_1 = -9.56$ and $\epsilon_2 = 0.31$ [27]. If the effective dielectric constant of the semiconductor structure $\epsilon_D = 3.5$ (the average between the dielectric constants of the semiconductor substrate and vacuum), then in the first approximation neglecting the effect of antenna width on surface plasmon-polariton wavelength λ_{pp} we obtain

$$\lambda_{pp} = \lambda_0[(\epsilon_1 + \epsilon_D)/\epsilon_1\epsilon_D]^{1/2} = 207 \text{ nm}. \quad (1)$$

This value is in good agreement with the oscillation period of γ found for antennas with $w = 200$ nm, which is an indication of the correct interpretation of the experimental results in terms of standing waves of hybrid surface plasmon-polariton modes. Here it is necessary to note that the condition of the formation of standing waves in any one-dimensional resonator is the integer number of half wavelengths; however, if the resonator works as an electric dipole antenna, the standing plasmon-polariton waves should create charges of opposite signs at the antenna ends. This condition is satisfied only for an even number of half wavelengths, so that the length L of one antenna arm is given by $L = 2N\lambda_{pp}$. This gives the period between the antenna resonances equal to λ_{pp}.

To verify the model, we investigated the effect of gold antennas on top of a quartz substrate with w of about 200 nm, using organic molecules (carotene, rhodamine, and other molecules) at wavelength $\lambda = 632.8$ nm. In this case $\epsilon_1 = -11.5$ and $\epsilon_2 = 1.3$ [27], and the effective dielectric constant of the structure $\epsilon_D = 2.5$. Analogous oscillations in γ were found in these studies with a period $L = 355$ nm corresponding to formula (1). Those results will be published elsewhere. Also note that the gold nanoantennas used to enhance emission from ZnSe/CdSe QDs resulted in almost zero amplification of the emission and no periodic oscillations of the amplification were detected. Such behavior is due to the fact that the absolute value of the dielectric constant ϵ_1 of gold at $\lambda = 488$ nm becomes substantially less than that of silver and no plasmon-polariton wave forms on the metal-semiconductor interface.

The simple formula (1) does not predict any dependence of λ_{pp} on antenna width and height. However, our measurements have revealed a weak dependence of the oscillation period on both w and h. This can easily be seen by comparing the dependences $\gamma(l)$ for antennas with $w = 200$ and 150 nm shown in Figs. 5 and 6, respectively. Both dependences show

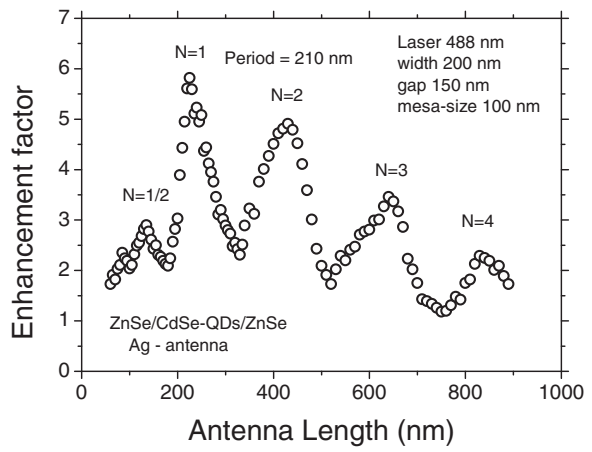

FIG. 5. Enhancement factor of the emission of QDs embedded in silver linear antennas ($w = 200$ nm and gap $D = 150$ nm) as a function of antenna length.

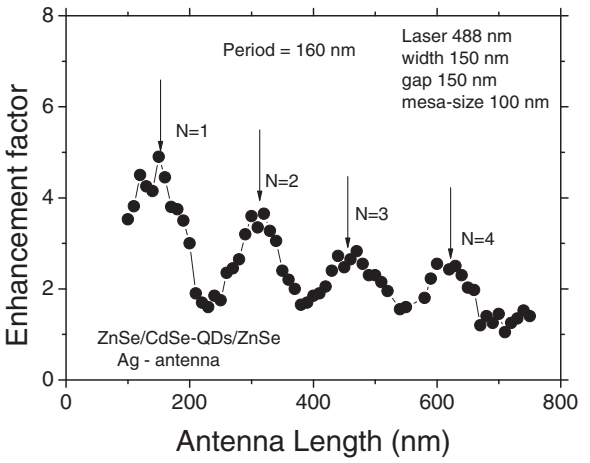

FIG. 6. Enhancement factor of the emission of quantum dots embedded in silver linear antennas (with $w = 150$ nm and gap $D = 150$ nm) as a function of antenna length.

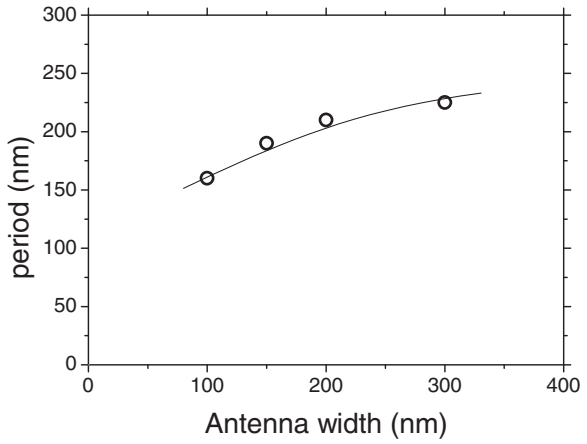

FIG. 7. Dependence of the oscillation period of the antenna enhancement factor on antenna width.

similar variations of the amplification ratio $\gamma(l)$, yet the oscillation period L for an antenna with $w = 150$ nm is 20% less.

The measured dependence of the oscillation period of the antenna amplification coefficient as a function of w is displayed in Fig. 7. It is seen that the oscillation period decreases by about 30% in the w range between 300 and 150 nm. A slight (∼15%) decrease of the oscillation period was also found as a result of the reduction of antenna thickness from 50 to 40 nm. The observed weak dependence of the phase velocity for the hybrid mode wave on the geometric parameters (width and thickness) of the antenna can be related to the variation of the components of the effective dielectric constant with changing antenna width and height, which should result in dispersion variations of the plasmon-polariton mode.

We have also studied the dependence of the enhancement factor on the gap width between the antenna stripes. This dependence is presented in Fig. 8, and it illustrates rather quickly the reduction of the antenna amplification with increasing gap, which corresponds approximately to dependence $[1 + (D_0/D)^2]$, with $D_0 = 300$ nm. This means

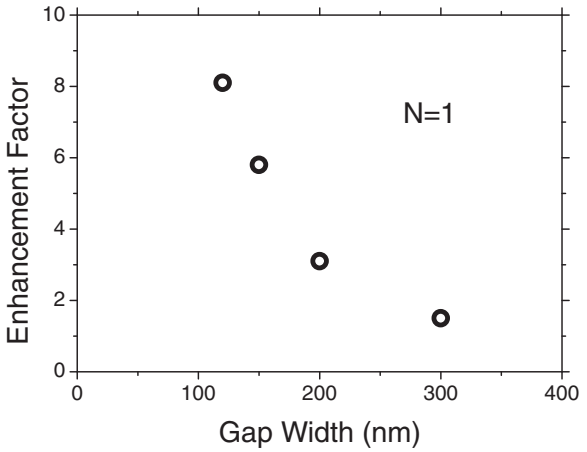

FIG. 8. Dependence of the enhancement factor on gap width, measured for an antenna width of 200 nm.

that enhancement of the electromagnetic field amplitude at small D follows $\sim 1/D$.

IV. NUMERICAL SIMULATION OF LINEAR ANTENNAS

We have numerically simulated properties of linear silver antennas using the finite-difference time-domain method (FDTD) [28] with the differential approach, which extends the FDTD method for a linear dispersive medium with a frequency-dependent dielectric constant [29] defined by

$$\epsilon(\omega) = \epsilon_\infty - \frac{(\omega_p)^2}{\omega(\omega - i\nu_p)}, \tag{2}$$

where ω_p is the plasma angular frequency and ν_p is the frequency of electron collision. In order to fit the dielectric constant of silver at a wavelength of 632.8 nm (with a corresponding frequency of 615 THz), according to Ref. [27], we took $\epsilon_\infty = 3.7$, $\omega_p = 1.41 \times 10^{16}$ s^{-1} and $\nu_c = 9 \times 10^{13}$ Hz. After Fourier transformation field components at a frequency of 615 THz were considered. In the numerical model the antenna made of silver was immersed in a homogeneous background medium with the dielectric constant value ϵ_D close to that of the boundary between vacuum and the semiconductor substrate. All the boundary faces of the calculation domain were equivalent to the perfectly matched layer. Since amplification of the local-field intensity by the antenna is directly related to the Purcell factor, we have expressed the results of numerical simulations in terms of a local-field intensity enhancement (LFIE) factor. This parameter is the enhancement of the E-field intensity in the antenna gap compared to the intensity of the incident planar wave.

Figure 9 shows periodic dependencies of the LFIE factor versus length L simulated numerically for $w = 140$ nm, $\epsilon_D = 2$, and gap width $D = 60$ and 70 nm. The inset in Fig. 9 maps

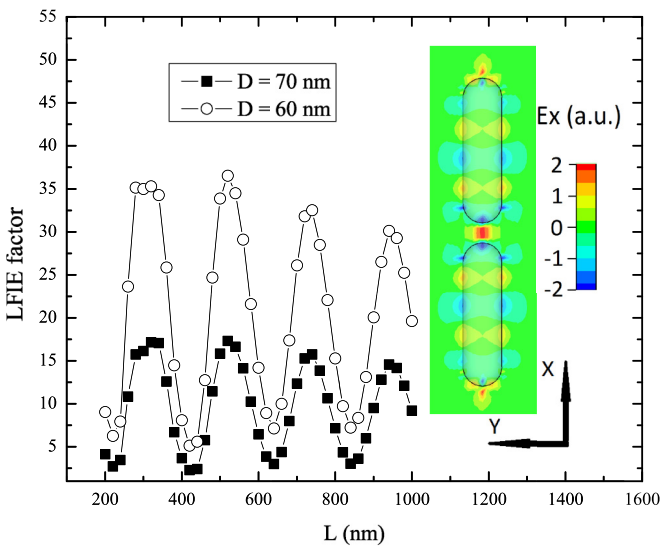

FIG. 9. (Color online) Numerically simulated dependence of the LFIE factor at a frequency of 615 THz as a function of the antenna length L for $w = 140$ nm, $\epsilon_D = 2$, and different gap sizes, $D = 60$ nm (line with squares) and $D = 70$ nm (line with circles). The inset shows the instantaneous distribution of the E-field x component for $L = 520$ nm.

out an instant distribution of Ex (the x component of the E field) at an excitation frequency of 615 THz for $L = 520$ nm, which corresponds to the second peak of the LFIE factor. On this map one can clearly see an odd number of periodic loops of Ex with alternating polarity. They are clear evidence of the existence of hybrid plasmon polaritons with the wave vector directed along the antenna. These waves propagating along the surface of the antenna stripes explain the nature of the periodic resonances in linear antennas. Each antenna arm has peaks of Ex with the same polarity at opposite ends, which is equivalent to the existence of charges with opposite signs there. This results in opposite charges on the antenna gap edges and on the opposite antenna tips. The former allows us to create a localized plasmon in the gap coupled to quantum dots, while the latter makes the combination of two nanostripes equivalent to an electric dipole antenna. Thus, the localized gap plasmon is coupled to the distributed plasmonic resonators that are the antenna arms guiding hybrid surface plasmon-polariton waves. Thus, the E field in the antenna gap is strongly affected by the distributed plasmonic resonators that are the antenna arms made of nanostripes guiding hybrid surface plasmon-polariton waves. One can also see periodic antinodes of Ex along the lateral edges of stripes related to the excitation of wedge plasmons [30] with the phase velocity slightly different from that of the surface plasmon polaritons. Wedge plasmons appear to have some influence on the E field in the antenna gap. A more detailed analysis of this complicated plasmonic multiresonant system will be presented in another publication. A low dielectric constant of the surrounding medium results in lower attenuation of the surface plasmons associated with a higher Q factor of the antenna arm resonances and therefore increases the LFIE factor. Numerical simulations with $\epsilon_D = 2$ demonstrated enhancement of the local-field intensity as high as 35 times. However, narrow antenna strips of width $w = 140$ nm significantly reduced the phase velocity of the propagating plasmon polaritons, so that the distance between the adjacent peaks of the LFIE factor (the period) was 220 nm.

V. EFFECT OF HELICAL ANTENNAS

Another interesting question is related to the feasibility of creating a selective optical nanoantenna, which amplifies only one of the two components of circularly polarized light. The key idea is based on induced asymmetry of the antenna: a curved antenna could have either right or left helicity. To solve the problem, we investigated the emission properties of ZnSe/CdSe QDs embedded in right- and left-oriented curved silver antennas. Since significant amplification by optical nanoantennas can be achieved only with a minimized antenna gap, we used two-leaf (S- and Z-like) chiral structures instead of a conventional four-leaf gammadion-like structure.

The characteristic fabricated structures with antennas with left and right helicity are shown in Fig. 10. A comparison of the emission properties of the 80-nm mesas with QDs embedded in nanoantennas with opposite (S and Z) helicity revealed a pronounced polarization dichroism with respect to photoexcitation induced by circularly polarized light.

The antennas with the clockwise and counterclockwise helicity enhance the photoexcitation efficiency of only the left- and right-circularly polarized light, respectively, just as

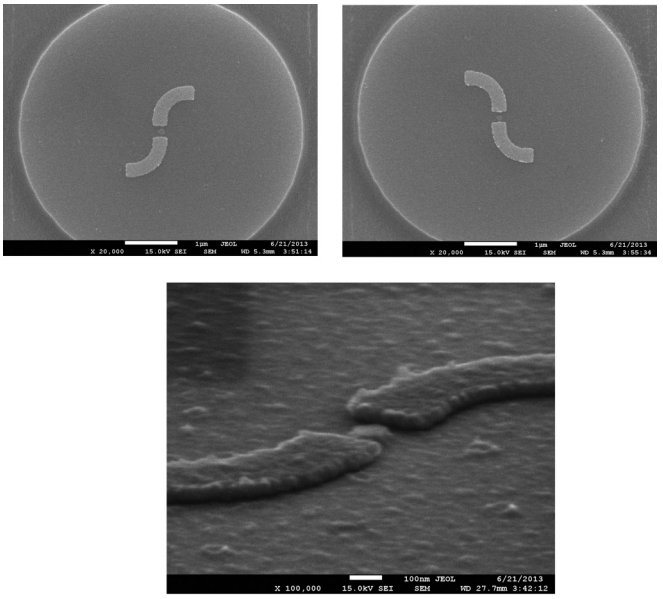

FIG. 10. Typical photos of the studied structures with curved antennas with clockwise and counterclockwise helicity.

the linear nanoantennas enhance the photoexcitation efficiency of the light linearly polarized along the antenna. This effect is illustrated in Fig. 11, which shows the emission spectra measured for mesas with ZnSe/CdSe QDs embedded in 400-nm-long curved antennas with opposite helicity (S and Z types) measured under left- and right-circularly polarized laser light (wavelength of 488 nm).

Figure 11 shows clearly that the integral emission intensities of the mesas embedded in curved antennas depend on the sign of circular polarization of photoexcitation. The emission intensities I_S^+ and I_S^- (I_Z^+ and I_Z^-) recorded under the excitation of S-like (Z-like) antennas with right (+) and left (−)

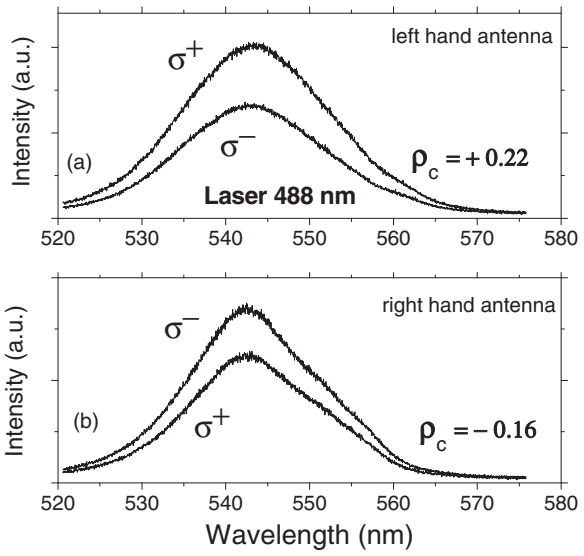

FIG. 11. Emission spectra measured for mesas with CdSe/ZnSe QDs embedded in 400-nm-length curved antennas with opposite helicity measured under (a) left- and (b) right-circularly polarized laser light (wavelength of 488 nm).

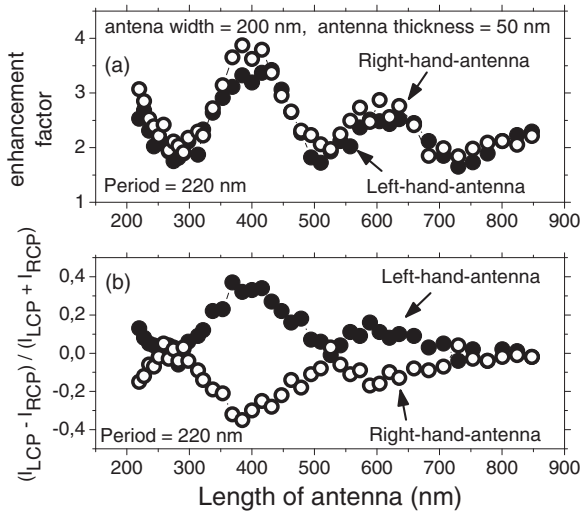

FIG. 12. (a) Enhancement factor of the emission of QDs embedded in curved antennas (with $w = 200$ nm, gap $D = 150$ nm) as a function of antenna length. (b) Strength of the selective polarization dichroism effect induced by photoexcitation with circular polarization as a function of the length of curved antennas.

circularly polarized light, respectively, differ from each other by about 20%, with the excitation efficiency being higher when the circular polarization of the exciting pulses coincides with the antenna helicity. It is important that such selective amplification does not occur at all antenna length values of curved antennas and occurs only at certain length ranges.

Figure 12 presents the measured dependences of emission intensities for mesas in the dominating circular polarization, i.e., I_S^+ and I_Z^-, and the degree of circular polarization $\rho_{c,i} = (I_i^+ - I_i^-)/(I_i^+ + I_i^-)$ for $i = S, Z$ on antenna length. It is seen that I_S^+, I_Z^-, ρ_{cs}, and ρ_{cz} are strongly dependent on antenna length and that all the dependences have an oscillating character. The maxima in $\rho_{c,i}(l)$ occur at the same $l \sim 380$ and 600 nm as in $I_S^+(l)$ and $I_Z^-(l)$, and the values of $\rho_{c,S}$ and $\rho_{c,Z}$ have opposite signs but similar amplitudes. Note that at given equal width (200 nm) and thickness (50 nm) of the metallic antenna the periods of the above oscillations appear to be very close in S- and Z-like antennas, namely, $L = 220 \pm 10$ nm, which, in turn, is very close to the period observed in the 200-nm-wide linear antennas equal to 210 ± 10 nm. This fact suggests that the main physical reason for the discovered resonances in emission amplification is the same as that for selective polarization dichroism, namely, formation of standing plasmon-polariton waves in metallic nanoantennas.

VI. CONCLUSION

We have studied optical nanoantenna-induced enhancement of photoexcited emission of ZnSe/CdSe QDs. Oscillations of the enhancement factor as a function of antenna length have been established, and it has been demonstrated that the period of the observed oscillations corresponds to the wavelength of the surface plasmon-polariton mode propagating in the metallic antenna. This interpretation of the experimentally observed periodicity has been confirmed by numerical simulations. The influence of the helicity of curved antennas on the amplification of the degree of circular polarization of photoexcitation has been investigated, and periodic amplification of the degree of circular polarization due to surface plasmon-polariton modes has been detected.

ACKNOWLEDGMENTS

We are grateful to I. Akimov, L. Kuipers, and R. Oulton for fruitful discussions. This work was supported by EU project SPANGL4Q.

[1] K. C. Gupta and A. Benalia, *Microstrip Antenna Design*, Artech House Microwave Library (Artech House, Norwood, MA, 1988).
[2] F. Gustrau, *RF and Microwave Engineering: Fundamentals of Wireless Communications* (Wiley, Hoboken, NJ, 2012).
[3] Y. W. C. Cao, R. C. Jin, and C. A. Mirkin, Science **297**, 1536 (2002).
[4] S. Nie and S. R. Emory, Science **275**, 1102 (1997).
[5] E. M. Purcell, H. C. Torrey, and R. V. Pound, Phys. Rev. **69**, 37 (1946).
[6] G. W. Ford and W. H. Weber, Phys. Rep. **113**, 195 (1984).
[7] I. A. Larkin, M. I. Stockman, M. Achermann, and V. I. Klimov, Phys. Rev. B **69**, 121403(R) (2004).
[8] K. J. Russell, T.-L. Liu, S. Cui, and E. L. Hu, Nat. Photonics **6**, 459 (2012).
[9] J. T. Choy, B. J. M. Hausmann, T. M. Babinec, I. Bulu, M. Khan, P. Maletinsky, A. Yacoby and M. Lončar, Nat. Photonics **5**, 738 (2011).
[10] K. Kneipp, Y. Wang, H. Kneipp, L. T. Perelman, I. Itzkan, R. R. Dasari, and M. S. Feld, Phys. Rev. Lett. **78**, 1667 (1997).
[11] R. D. Grober, R. J. Schoelkopf, and D. E. Prober, Appl. Phys. Lett. **70**, 1354 (1997).
[12] T. H. Lee, *Planar Microwave Engineering: A Practical Guide to Theory, Measurement, and Circuits* (Cambridge University Press, Cambridge, 2004).
[13] S. M. Sze, *Physics of Semiconductor Devices* (Wiley, New York, 1981).
[14] M. S. Tyagi, *Introduction to Semiconductor Materials and Devices* (Wiley, New York, 1991).
[15] P. J. Bulman, G. S. Hobson, and B. C. Taylor, *Transferred Electron Devices* (Academic, New York, 1972).
[16] E. Yablonovitch, Phys. Rev. Lett. **58**, 2059 (1987).
[17] S. John, Phys. Rev. Lett. **58**, 2486 (1987).
[18] J. Joannopoulos, R. Meade, and J. Winn, *Photonic Crystals* (Princeton University Press, Princeton, NJ, 1995).
[19] P. Muhlschlegel, H.-J. Eisler, O. J. F. Martin, B. Hecht, and D. W. Pohl, Science **308**, 1607 (2005).
[20] S. V. Ivanov, A. A. Toropov, T. V. Shubina, S. V. Sorokin, A. V. Lebedev, I. V. Sedova, P. S. Kop'ev, G. R. Pozina, J. P. Bergman, and B. Monemar, J. Appl. Phys. **83**, 3168 (1998).

[21] D. P. Fromm, A. Sundaramurthy, P. J. Schuck, G. Kino, and W. E. Moerner, Nano Lett. **4**, 957 (2004).
[22] P. J. Schuck, D. P. Fromm, A. Sundaramurthy, G. S. Kino, and W. E. Moerner, Phys. Rev. Lett. **94**, 017402 (2005).
[23] W. L. Barnes, A. Dereux, and T. Ebbesen, Nature (London) **424**, 824 (2003).
[24] A. Sommerfeld, Ann. Phys. (Berlin, Ger.) **28**, 665 (1909).
[25] H. Morawitz, Phys. Rev. **187**, 1792 (1969).
[26] A. Adams, R. W. Rendell, W. P. West, H. P. Broida, P. K. Hansma, and H. Metiu, Phys. Rev. B **21**, 5565 (1980).
[27] P. B. Johnson and R. W. Christy, Phys. Rev. B **6**, 4370 (1972).
[28] K. S. Yee, IEEE Trans. Antennas Propag. **14**, 302 (1966).
[29] R. Joseph, S. Hagnes, and A. Toflove, Opt. Lett. **16**, 1412 (1991).
[30] E. Moreno, S. G. Rodrigo, S. I. Bozhevolnyi, L. Martín-Moreno, and F. J. García-Vidal, Phys. Rev. Lett. **100**, 023901 (2008).